Chapter 1

Sediment Transport Dynamics in Ports, Estuaries and Other Coastal Environments

X. H. Wang and F. P. Andutta

Additional information is available at the end of the chapter

http://dx.doi.org/10.5772/51022

1. Introduction

Given ever expanding global trade, the international economy is linked to the well-being of major coastal infrastructures such as waterways and ports. Coastal areas comprise about 69% of the major cities of the world; therefore the understanding of how coastal aquatic environments are evolving due to sediment transport is important. This manuscript discusses topics from both modelling and observation of sediment transport, erosion and siltation in estuarine environments, coastal zones, ports, and harbour areas. It emphasises particular cases of water and sediment dynamics in the high energy system of the Po River Estuary (Italy), the Adriatic Sea, the Mokpo Coastal Zone (South Korea), the Yangtze Estuary and the Shanghai Port, the Yellow Sea (near China), and Darwin Harbour (Northern Australia). These systems are under the influence of strong sediment resuspension/deposition and transport that are driven by different mechanisms such as surface waves, tides, winds, and density driven currents.

The development of cities around ports is often associated with the expansion of port activities such as oil, coal, and gas exportation. Such development results in multiple environmental pressures, such as dredging to facilitate the navigation of larger ships, land reclamation, and changes in the sediment and nutrient run-off to catchment areas caused by human activities [1]. The increase in mud concentrations in coastal waters is a worldwide ecological issue. In addition, marine sediment may carry nutrients and pollutants from land sources. An understanding of sediment transport leads to a better comprehension of pollution control, and thus helps to preserve the marine ecosystem and further establish an integrated coastal management system [e.g., 2-3]. [4] observed that many historical sandy coasts have been replaced by muddy coasts, and is considered permanent degradation. Additionally, [5] reported that recreational and maritime activities may be adversely impacted by

processes of sediment resuspension and deposition. It was shown by [6] that increased sediment concentration in the Adriatic Sea has affected the growth of phytoplankton at the subsurface, because sunlight penetration is considerably reduced.

Before proceeding with the key issues about the transport of sediment in the previously mentioned systems, a brief and summarized overview of the main characteristics and dynamics of sediment transport is provided to contribute to the understanding of this chapter. In general, sediment particles considered in transport of sediment cycle, consist of non-cohesive and cohesive sediment types (Fig. 1a). (a) Sediments of particle size d_{50}< 4 μm, mud or clay, are classified as a cohesive sediments. In contrast, (b) particle size d_{50}> 64 μm may be weakly cohesive; however, these particles are included in the non-cohesive group, and range from mud through to sand [7]. The dynamics of sediment transport rely upon water circulation, salinity concentration, biological interaction, and sediment type. Cohesive sediments, such as clay and small-particle mud, are often transported in the water column, as these sediments are easily suspended by water currents. Alternatively, non-cohesive sediments, such as sand, are usually transported along the bottom by the processes of saltation, rolling, and sliding. Many numerical models include these processes and are based on empirical experiments, often performed in laboratories. These experiments provide estimates of the bed load transport according to particle size, bottom stress, and a threshold stress for initial bed movement [7].

The interaction between sediments is also an important feature pertinent to the transport of sediment. The interaction among cohesive sediments (mud) is different from that of non-cohesive sediments (sand). Cohesive sediments may aggregate, forming flocs of typical sizes of 100-200 μm. This aggregation process is called flocculation, and is caused by chemical or biological interaction. Flocculation is important for increasing the settling velocity; flocculated sediment particles settle faster on the bottom. "*Chemical flocculation*" is started by salinity ions that attach to the small mud particles, causing electronic forces between these particles, which start aggregating and thus forming a larger mud floc. In contrast, "*Biological flocculation*" is caused by bacteria and plankton, which produce exopolymer (i.e. a transparent mucus) that acts as glue between mud particles. This mucus results in the formation of extremely large flocs (~1000 μm in size), known as snow flocs [7].

The concentration of sediment near the surface may affect the formation of snow flocs, because sunlight penetration in the water column is decreased due to increased suspended-sediment concentration (SSC) and thereupon the reduced light penetration inhibits the production of plankton. In high turbidity waters, i.e. SSC > 0.5 g l^{-1}, marine snow is scarce; however, in less turbid water, i.e. SSC < 0.1 g l^{-1}, marine snow is common. Also, algae mats formation may influence the degree of erosion, because they decrease the propensity of sediment resuspension. In contrast, the influence of animal burrows may facilitate erosion [7]. Because of the different types of sediments and the flocculation process, the profile of the vertical distribution of SSC varies considerably. This vertical profile may indicate a well-mixed distribution, a smooth increase in sediment concentration with depth, or a depth-increase concentration with a step shape, called lutocline (Fig. 1b). The lutocline inhibits vertical mixing and thus conserves a nepheloid layer (i.e. bottom layer of high sediment concentration).

http://dx.doi.org/10.5772/51022

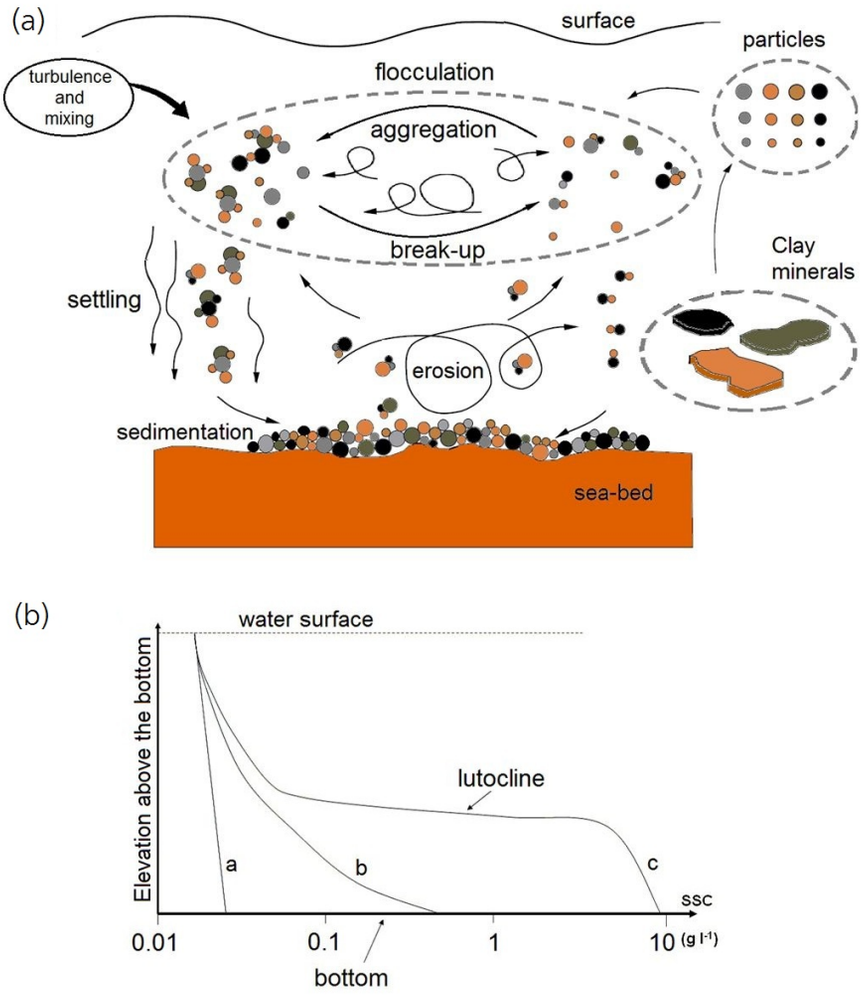

Figure 1. (a) Cycle of deposition and resuspension of cohesive sediment involved in particle aggregation and breakup. (b) Three typical vertical profiles of suspended sediment concentration in estuaries, where a, b and c denote a nearly well-mixed, partially-mixed and step shape profiles, respectively [source: 7-8].

This chapter gives an overview of four important suspended sediment transport processes that occur in ports, estuaries and other coastal environments. The following topics are investigated, based upon research on sediment dynamics at the University of New South Wales, Australia:

- The importance of including wave-currents when modelling sediment transport, showing the effect of waves generated during Bora events on SSC and net sediment flux in the Northern Adriatic Sea;
- The effect of increased SSC, combined with increased irradiance factor (Fc) of photosynthetically active radiation (PAR), on phytoplankton blooms (PB), with analysis of the PB event that occurred between January and April 2001 in the Mokpo Coastal Zone (Korea);
- The effect of coastal constructions on sediment transport, with analysis of the effect of dikes on the Yangtze River Delta, and problems with silting in the navigation channel of Shanghai Port (China);

- Tidal circulation modelling, specifically the role of mangrove and tidal flat areas in causing tidal asymmetry, and the effect on the transport of suspended sediment in Darwin Harbour (Australia).

2. Description of study sites

2.1. The Po River and the Adriatic Sea

The Po River (~12.5° E and ~45° N) is 680 km in length, and is located in the northern area of the Adriatic Sea. It provides up to 50% of the total fresh water discharge into the Adriatic Sea (Fig. 2). The annual mean river flow is ~ 46 km^3/year, with the maximum river discharge events typically occurring during the spring and a few times in autumn. The climate is temperate, with average temperatures of over 10° C in summer, and over 0° C in winter, and a runoff of 250-750 mm/year. Strong northeasterly winds prevail in winter, known as Bora events (typical wind speed ~30 m s^{-1}). These winds are usually ~10 ° C cooler than the water in the Adriatic Sea. In contrast, the southeasterly winds, which are often less intense and occur during summer and autumn, are known as Scirocco. The Bora and Scirocco wind conditions result in downwelling and upwelling events, respectively, in the western Adriatic coast [9-11].

The Adriatic Sea is a semi-enclosed sea, being one of the arms of the Mediterranean Sea. The Adriatic is connected to the eastern part of the Ionian Sea through the Ontranto Strait (Fig. 2). This sea is approximately 800 km long and 200 km wide. Depths vary from less than 200 m in the northern area, up to 1320 m in the southern area – with such depths covering an entire ~120 km wide expanse (i.e. South Adriatic Pit, [12]), and reduce to less than 800 m at the 70 km wide Ontranto Strait [10]. The eastern coast of the Adriatic Sea comprises numerous islands varying in main diameter from a few tens of meters up to tens of kilometres, and this coastline has many zones of high steepness. In contrast, the western coast has isobaths running parallel to the coastline and a smoother slope compared to the eastern coast (Fig. 2). The Adriatic Sea receives the runoff of 28 rivers, mostly located along the coast of Italy. The main river inflow to the Adriatic is from the Po River; however, the rivers Tagliamento, Piave, Brenta, and Adige together contribute a runoff of ~15.2 km^3/year, which is nearly one third of the Po's total runoff. The remaining 23 rivers in the Adriatic provide an average runoff of ~8 km^3/year [11].

The general circulation in the Adriatic Sea has been studied using field data and numerical simulations by [1, 10, 13-16], and is observed to be a cyclonic (anti-clockwise) circulation that is highly variable with the seasons [10, 13-17]. The annual water temperature excursion exceeds 15° C. [1] observed the intense boundary current on the western side, the Western Adriatic Coastal Current (WACC), which is both thermohaline and wind driven. The WACC reaches maximum velocities during winter, under the influence of strong northeasterly wind stress, i.e. Bora events [18]. The thermohaline component of the WACC is mainly forced by river discharge from the Po River, and thus reaches maximum intensity during spring and autumn [9, 19]. The position of the WACC is deflected from the inshore areas in winter, towards the shelf slope during the summer by an opposite wind-driven current due

http://dx.doi.org/10.5772/51022

to Scirocco events. Similar processes showing boundary currents being pushed offshore by opposing wind-driven currents have also been observed at other shelves, such as: the Great Barrier Reef, the continental shelf north of the Monterey Bay, and New Jersey shelf [20-22].

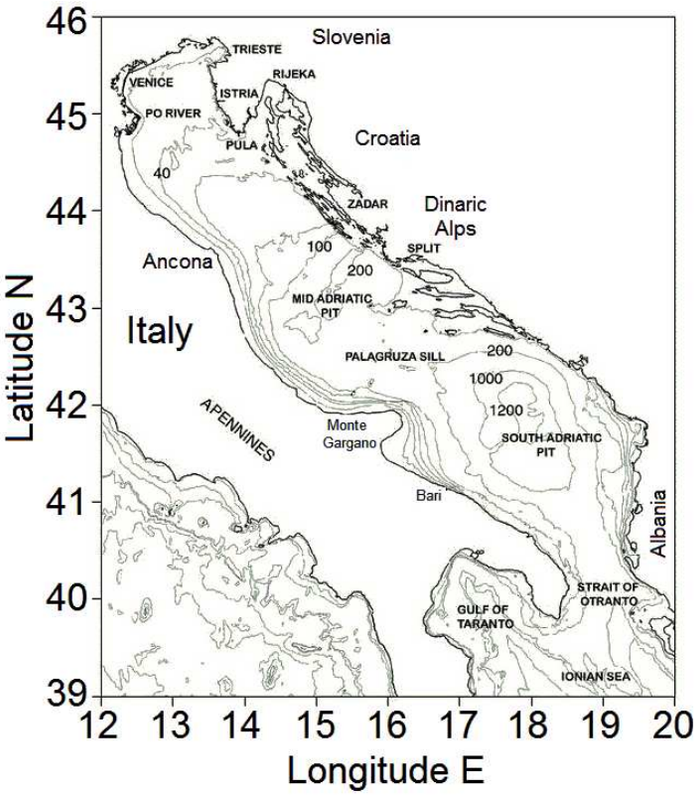

Figure 2. The Adriatic Sea location and a synthesized description of the main circulation.

Thermal balance in the Adriatic Sea is complex and influenced by river discharge (e.g. the Po River), surface heat flux by the wind (Bora and Scirocco events), and heat flux through the Otranto Strait. Water masses of the Northern Adriatic are renewed each year when the colder and denser water mass sinks and moves along the seabed to the deep basin of the Adriatic [1]. This northern Adriatic water mass forms a "*denser cascade water*", which, for the Adriatic Sea, is caused by temperature gradients, while for many aquatic systems, located in Tropical and Sub-tropical areas, this is often caused by hypersaline waters [e.g. 23-30]. During the spring and summer, however, the water mass in the northern Adriatic is warmed up and forms a well-defined thermocline. Furthermore, the water discharge from the Po River is an important controlling factor to the baroclinic currents in the basin of the Adriatic Sea [9]. The thermal balance within the Adriatic Sea is also maintained by the net heat inflow through the Otranto Strait from the Ionian Sea [1].

The annual load of sediment from the Po River is 10-15 x 10^6 tons/year. The sediment in the Northern Adriatic Sea is mainly formed by sand with grain size varying from 50 to 2000 μm, and silt with grain size between 2 and 50 μm. The smaller sediment particles, i.e. clay, are also observed, however, they do not provide the major contribution of fine sediment in the

northern area [1]. This chapter concerns the sediment transport in the Adriactic Sea of two classes: sediment particles larger and smaller than 50 μm grain size. [31] suggested that fine sediments such as silt and clay are mostly supplied from the Northern Adriatic Sea Rivers (e.g. Po River). Sediment is supplied into the sea and later dispersed through local circulation. Because the general circulation of the Northern Adriatic Sea is cyclonic, with the presence of the WACC on the western coast, there is a possibility that the sediment input from the rivers in the Northern Adriatic is transported southward by the coastal current. Therefore, the bottom sediment distribution would be predominantly sorted by the grain size according to their respective settling velocities.

2.2. The Youngsan River and the Mokpo Coastal Zone (Korea)

The Youngsan River Estuary (YRE) is located in the Mokpo coastal zone (MKZ), in the southwestern area of South-Korea (Fig. 3). The annual mean river flow is ~1.5 km^3/year, and the sediment load to the Yellow Sea is 0.7 x 10^6 tons/year. The climate is temperate, with average temperatures typically between 1.7° C and 4.4° C during winter and between 21.4° C and 26.1° C in summer. Maximum rainfall generally occurs during summer, accounting for 50 to 70% of the annual precipitation. Annual runoff is 250-750 mm. [11, 32-33]. The Mokpo area is located at the southeastern boundary of the Yellow Sea, and the YRE is connected to the Yellow Sea through four narrow inlets (i.e. ~1-3 km wide).

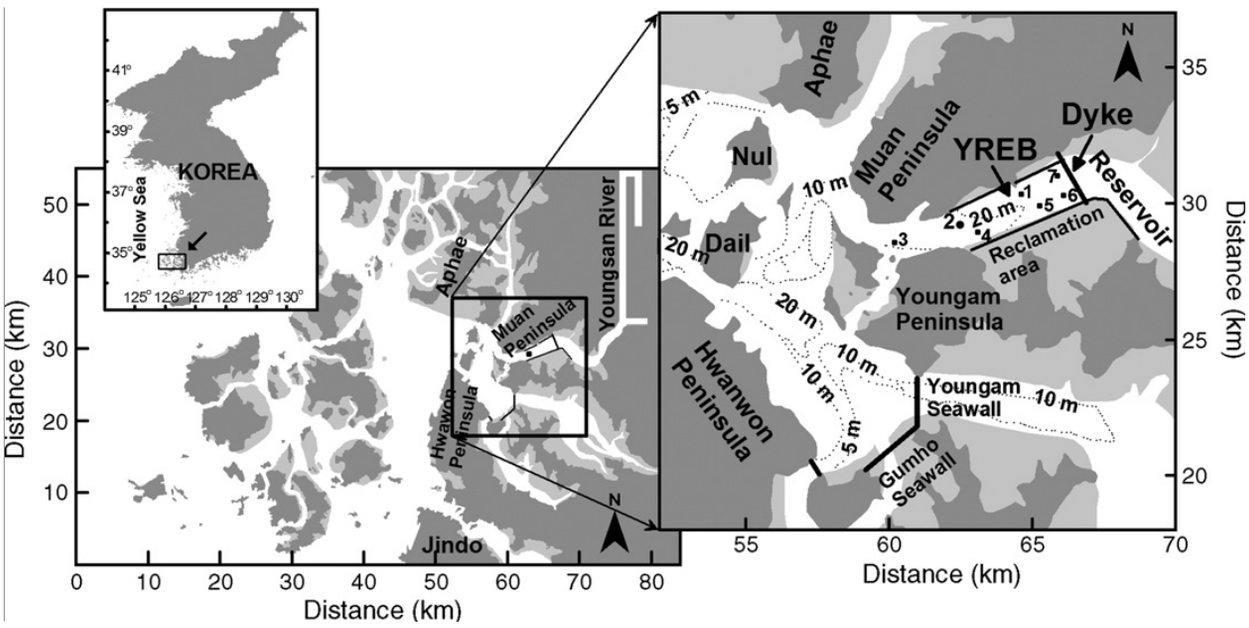

Figure 3. The domain of the hydrodynamic-sediment transport model at the southwest coast of Korea. The inset shows the location of the 1-D ecosystem model (●) in the Youngsan River Estuarine Bay (YREB) [source: 33].

Tidal features in the YRE are mixed, but predominantly semidiurnal according to the criteria of A. Courtier of 1938 [34], with the tidal form number [$N_f=(K_1+O_1)/(M_2+S_2)=0.28$]. Although there is the presence of many island and tidal flat areas, the tidal currents of the YRE are ebb dominant. Ebb/flood dominance is characterized by a shortened ebbing/flooding period, resulting

in stronger ebb/flood currents, respectively. In addition, the flooding periods are nearly twice as large as the ebbing periods [35-37]. The ebb dominance is likely to be caused by important features such as the many scattered islands, combined with the extensive tidal flats [35]. Moreover, [38] observed that ebb dominance is likely to appear in regions of abundant tidal flats.

To add complexity to such tidal asymmetry problems (e.g. flood and ebb dominance), the MCZ has three important sea structures: the dike built in 1981, the Youngam seawall built in 1991, and the Geumho seawall built in 1994. Since the construction of these structures, changes in the tidal characteristics such as the increased amplitudes have been observed [37, 39-40].

This chapter section aims to show that in order to properly predict the variability in phytoplankton mass production in the turbid waters of the MCZ, it is important to use a 3D sediment transport model, coupled with the ecosystem model. This solves the variable vertical dynamics of sediment resuspension and mixing [33].

2.3. Yangtze River and the Shanghai Port in the East China Sea

The Yangtze River or Changjiang River (Fig. 4) is the third longest river in the world (6300 km), and the fourth in terms of both water flow (~900 km^3/year) and sediment discharge (470-490 x 10^6 tons/year), with the transport of a dissolved load of 180 x 10^6 tons/year [11, 41-44]. The climate of this area is temperate, with temperatures of over 10^o C in summer and 0^o C winter, and an average runoff of 250-750 mm/year, the maximum river discharge occurring in summer [11]. The Yangtze is a mesotidal estuary according to the criteria of A. Courtier of 1938 [34], with a mean tidal range of 2.7 m [43].

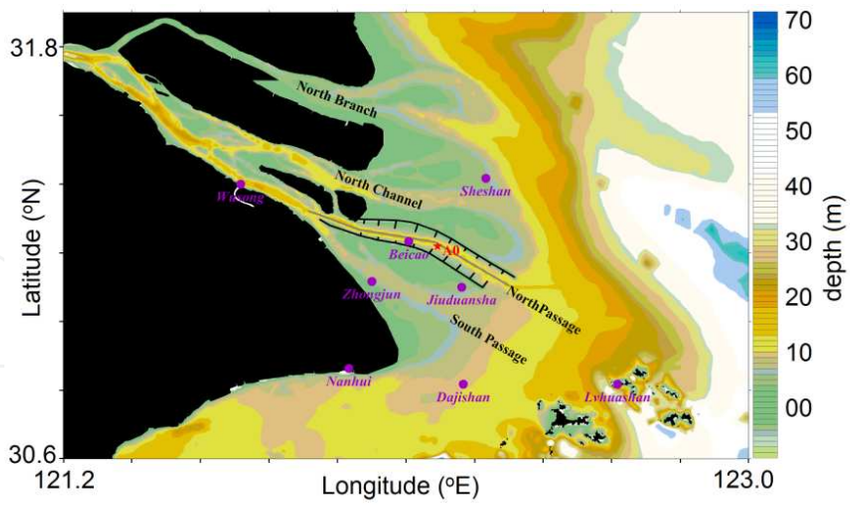

Figure 4. The Yangtze River or Changjiang River in China, and the indication of the navigation channel used for the trades of Shanghai Port [source: 44].

The sediment of the Yangtze River Estuary (YRE) mainly consists of small sediment particles of less than 63 μm (over 95%). The system is dominated by small sediment particles that lead to a highly turbid environment, and therefore the near bottom SSC can reach or exceed 4 g/l [44-47].

The Yangtze connects to the coastal zone through four inlets, namely North Branch, North Channel, North Passage, and South Passage. The main physical mechanics driving the transport of suspended sediment (TSS) varies between the four inlets: (a) in the South Passage TSS is mainly driven by tidal distortion, (b) in the North Passage TSS is dominated by gravitational circulation and tidal distortion, (c) in the North Channel TSS is dominated by gravitational circulation, and (d) for the North Branch the main mechanisms are not well described [44, 48-49]. For the North Passage other mechanisms are also suggested to contribute to the TSS and formation of the estuarine turbidity maximum zone (ETM), which include advective transport and turbulence suppression by salinity or suspended sediment induced stratification [50]. [51] performed a large analysis of the temporal and spatial variation of fluid mud, and flocculated settling. However, the joint contribution of the different TSS driving mechanisms with geometry is quite complex and requires further investigation.

The TSS in the Yangtze River Estuary (YRE) has been studied for many years [e.g. 41, 48-49, 52-59]. However, since the completion of the Deep Navigation Channel in 2011, important changes to the local hydrodynamics, and thus to the transport of sediment, are expected. In addition, there is the effect of the fluvial sediment trap by the Three Gorges Dam, which caused a significant decrease to fluvial sediment load [59-60]. Although the reduction of fluvial sediment has been reported, the silting problem attracted attention because the estimate deposition of sediment in the navigation channel was over 100% of the original yearly average predicted value, i.e. 30 million m^3 [62]. Recently, [44, 63] have reported that the greater siltation within the delta of the YRE is mostly influenced by the redistribution of local sediment through processes such as erosion and deposition within the delta area.

On Yangtze Estuary is the Shanghai Port, the world's busiest container port, which is extremely important to the economy of China. During 2010 and 2011, this port handled nearly 30 million container units per year. To facilitate local navigation, the Deepwater Navigation Channel (DNC) was built, 92 km in length and 12.5m deep. Although the channel comprises two dikes of nearly 50 km each, as well as 19 groins built to increase speed along the DNC, silting is still an issue, and dredging maintenance is greater than originally predicted [44, 55, 64-67].

A 1-DV model was applied to study the fine suspended sediment distribution at the South Channel-North Passage of the YRE [68]. Then, a 2D vertical integrated model was used to simulate, and subsequently to investigate the characteristics of tidal flow and suspended sediment concentration at this channel [69]. From these studies it was observed that new features had formed after the finalization of the shipping channel; however, the model used did not include the baroclinic component, which is an important factor in the transport of sediment.

2.4. Darwin Harbour (Australia)

Darwin Harbour (DH) is a shallow estuary, with a typical depth of less than 20 m and a maximum depth of up to ~40m. The harbour is situated in the Northern Territory (NT) of Australia, and connects to the Timor Sea. The land surrounding DH is occupied by the cities of Palmerston and Darwin (the latter is the capital of NT). DH is defined as the water body south of a line from Charles Point (west point) to Gunn Point (east point), and comprises the Port Darwin, Shoal Bay and the catchments of the West Arm, Middle Arm and East Arm

http://dx.doi.org/10.5772/51022

[Darwin Harbour Advisory Committee 2003]. DH forms two adjacent embayments. The western embayment receives the freshwater inputs predominantly from the Elizabeth River (flowing into the East Arm), the Darwin River, Blackmore River and Berry Creek (flowing into the Middle Arm), while the eastern embayment receives freshwater input from the Howard River [70]. DH area comprises numerous tidal flats and mangroves, with nearly 5% of the whole mangrove area in the Northern Territory, i.e. ~274 km^2. [71-72]

Darwin Harbour is forced by semi-diurnal tides, and is classified as a macro-tidal estuary (tidal form number Nf = 0.32). The maximum observed tidal range is 7.8 m, with mean spring and neap tidal ranges of 5.5 m and 1.9 m, respectively [11, 73-76].

Evaporation usually exceeds rainfall throughout the year, except during the wet season. From February to October, the evaporation rate ranges from 170 mm to 270 mm, respectively, with an average annual evaporation rate of ~2650 mm. The fresh-water input into DH is negligible in the dry season, and evaporation exceeds river discharge. Therefore, in the dry season salinity concentrations in the harbour may become at least 0.8 psu higher than the adjacent coastal waters [77].

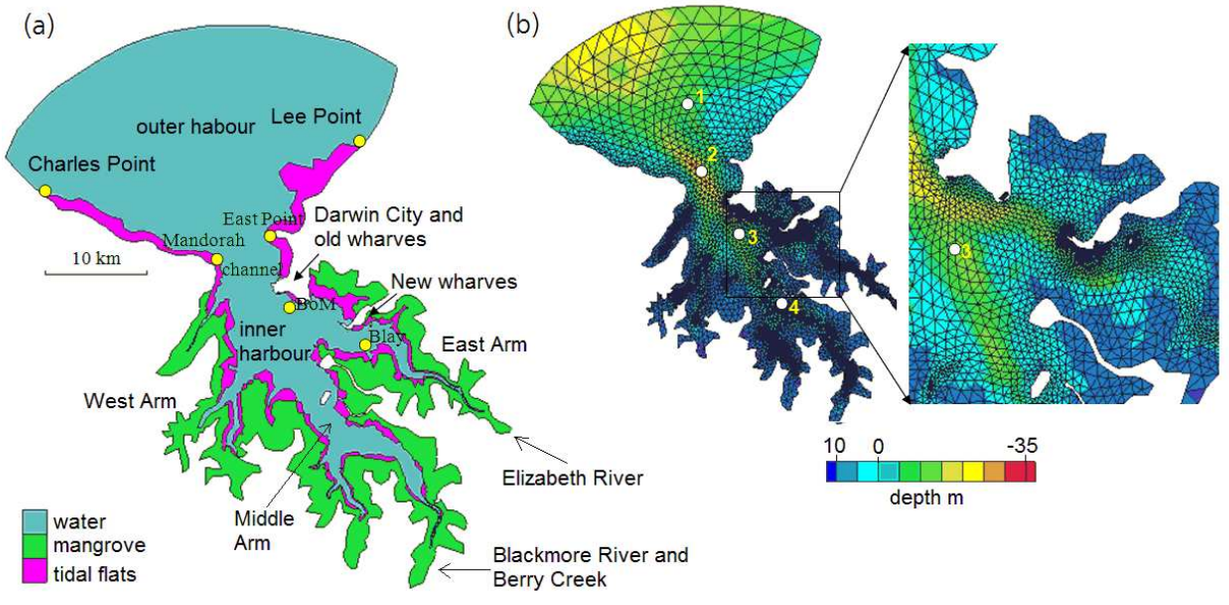

Figure 5. (a) Model domain of Darwin Harbour with indication of the harbour areas and data available to calibrate and validate the model (yellow dots). (b) Unstructured numerical mesh used for the simulations, where colour corresponds to depth in meters, and numbered points indicate location of sampling stations used to analyse tidal asymmetry along the harbour [source: 76].

The climate of this region is tropical savannah, with average monthly temperatures of over 20^o C throughout the year. DH is located in a subarid/humid area with a typical rainfall of 1500-1600 mm/year (rainfall of 2500 mm in exceptionally wet years). Runoff typically varies between 100 and 750 mm/year, with maximum runoff usually occurring between October and April [11]. Although DH is of great economic importance to the NT, most of the current knowledge about the main driving forces for the local hydrodynamics

is due to efforts by [75-76, 78-80]. To add complexity to the understanding of the hydrodynamical and morphological changes in DH, the combined effect from the headlands, rivers, and embayments create a complicated bathymetry that leads to the formation of many tidal jets within narrow channels, eddies etc.

[76] Conducted some research at the western embayment of DH (Fig. 5a), and provided a calibrated and validated model to study the hydrodynamics in the harbour (Fig. 5b). From this study, the role that the mangrove and tidal flat areas play on the tidal asymmetry could be verified. It was thus confirmed that a decrease in area of the tidal flat and mangroves would lead to increased tidal asymmetry of flood dominance, and, because of this, result in the net sediment transport to the inner harbour area.

3. Methods

This chapter addresses the different study regions, followed by independent research and numerical modelling. As such, we have provided the methodology in separate sub-sections. Each of the following sub-sections summarizes the field work conducted, the calibration, and validation of the model for the four study sites.

3.1. Setting up of the numerical model for the Northern Adriatic Sea

For the Adriatic Sea, a sediment transport model similar to that of [81] was used, with improvements made by incorporating the effect of wave current [1, 82-84]. The Adriatic Intermediate Model was based on the Princeton Ocean Model (POM) [85]; with the horizontal resolution of 5 km applied to a structured mesh. The model had 21 vertical layers that used the sigma coordinate, with a high vertical resolution was used near the surface and bottom. The simulations had the time steps of 7 and 700 seconds for the external and internal modes. The 2.5 turbulent closure method of Mellor-Yamada was used, and the diffusivity coefficient for SSC was assumed to be equal to that of heat and salt, and viscosity according to [86].

The flocculation of fine suspended sediment is mostly observed near the Po River mouth, and in areas before reaching the ocean [87]. Because of that, flocculation or aggregation processes were neglected, and thus all sediment behaves as a non-cohesive type and moving as a Newtonian fluid. For the fine sediment, i.e. silt and fine sand ($20 < d < 60$ μm), resuspension was caused by turbulence. Inertia of sediment particles was also neglected, and their vertical velocity parameterized by a small settling velocity (w_s). For more information about the settling velocity, sediment source in the Adriatic Sea, and all the physical and numerical parameters used in the model, please refer to [1, 82-84].

The tides are known to be relatively week in the Northern Adriatic Sea; however, [83] included the tides to observe the tidal current effect on sediment transport. For the bottom stress two expressions were applied, an expression that considered the wave orbital velocity on the bottom, and the other expression that neglected this effect. The third version of the SWAN model was used to simulate the waves. The model was used in the stationary mode to compute the wave fields under the forcing of 6 hour interval.

http://dx.doi.org/10.5772/51022

The suspended sediment concentration was assumed not to affect water density. It is important to note that this last assumption is only valid for low concentrations of SSC, such as those lower than 1 g/l [e.g., 88-90]. The conservation of SSM in the water column was applied and the fluid considered incompressible. [2] showed that the Adriatic Sea is supplied by a riverine sediment input that is ~ 1.67 Mt/month, with the Po River contributing nearly 70% of that. The other rivers along the Adriatic coast had the equal contribution, which represented the remaining 30 % of the sediment input.

The sediment dynamics in the Northern Adriatic Sea is induced by riverine sources or resuspended sediment from the seabed. Simulations were conducted to quantify the different mechanisms responsible for the transport of suspended sediment [1], and the simulations examining in details the wave-current interaction [84].

The numerical simulations by [1] were: (a_1) simulation forced only by the Po River plume, (b_1) simulation forced by the Po River plume and wind stress. (c_1, d_1 and f_1) simulation forced by the Po River plume, wind stress, and additional wave forcing. For the simulation assuming wind effect, the assumed wind conditions were the Bora and Scirocco, which are typical wind conditions of the region [e.g., 9, 14-15, 19, 91] and summarized in [Table 2, in 1]. A homogeneous field with initial temperature of 12^o C, and salinity 38 psu were assumed in the model. These are representative of ambient winter conditions without stratification. Simulations for a 30 day period were made, assuming continuous discharge from the Po River.

In contrast, the numerical simulations by [84] were: (a_2) simulation forced without waves, tides, and SSC effect on water density; (b_2) simulation forced by waves, but without tides and SSC effect on water density; (c_2) similar to b_2, except with waves assumed to be aligned with bottom currents; (d_2) simulation forced with waves and tides, but without SSC effect on water density; (e_2) simulation forced with waves and SSC effect on water density, but without tides. River runoff was assumed to be continuous from 1 January 1999 to 31 January 2001. The initial conditions were obtained from climatological simulation of the Adriatic Sea circulation in [17], and the sediment model was coupled with the hydrodynamical model from 1 December 2000.

3.2. Setting up of the numerical model for the Mokpo Coastal Zone

The simulation for MCZ consists of a 3D hydrodynamical model coupled with the sediment transport model, and a 1-D biogeochemical model [33]. The Princeton Ocean Model (POM) was chosen [85]. This model used the 2.5 turbulence closure scheme [92], and included the effect of sediment concentration on water density, and the stability function on the drag bottom coefficient [93]. The biological 1-D Modular Ecosystem Model (MEM) is based on the European Regional Sea Ecosystem Model [94]. This model constrains the physical and geophysical environmental conditions such as photosynthetically active radiation, temperature, and salinity. It also includes the trophic interactions between biological functional groups [95-96].

The simulations were run from January to April 2001, and the vertical salinity and temperature data used to calibrate/validate the hydrodynamical model were obtained by Mokpo National University at seven stations in the Youngsan River Estuary. The period of simula-

tion partially covers the winter to spring seasons, and the distribution of the 7 sampling stations covers areas near the river mouth and upstream regions.

Hourly data from the hydrodynamic and sediment model were provided to the biogeochemical model. Specifically, temperature was used to compute the metabolic response to the biota, salinity was used for oxygen saturation concentration, the vertical diffusion coefficient was used for the biogeochemical-state variables, and the combination of sea surface elevation with suspended sediment concentration was used to estimate light penetration in the water column. The river discharge from the Youngsan Reservoir was also included. The water depth at the Youngsan River Estuarine Bay was assumed to be 21 m. The horizontal grid resolution of the model was 1km, with 18 vertical sigma layers. The open boundary was forced with the four main tidal components, i.e. M_2, S_2, K_1 and O_1. Nodal corrections and astronomical arguments were included to predict tides during the period of simulation.

The initial concentration values of pelagic biogeochemical are listed in (Table 1). The phytoplankton population, biomass content of carbon, nitrogen, phosphorus, and silicon for each phytoplankton group were obtained from [97]. Model sensitivity tests were performed in 8 different simulations, by assuming different parameters for light attenuation and vertical mixing rates, see Table 4 in [33]. A complete description of the whole setting of the model, the modelling experiments, and additional numerical and physical parameters is provided in [33].

	Nitrate	Phosphate	Ammonia	Silicate	DO
Surface	2.25	0.26	1.15	6.02	333
Bottom	1.36	1.20	1.20	7.36	340

Table 1. Initial condition assumed for concentrations of pelagic biogeochemicals (unit in mmol m^{-3}) [source: 33].

3.3. Setting up of the numerical model for the Yangtze Estuary

To study the hydrodynamics and transport of sediment, the 3D Princeton Ocean Model (POM) was used. This model uses a structured mesh and resolves the equations for momentum, temperature, and salinity using the finite differences method. The vertical coordinate is sigma [85, 98-99], and the turbulent closure method is described in [92, 100], while to compute the vertical mixing processes [101] was used. To compute the horizontal diffusion of momentum, the Smagorinsky diffusion scheme [86] was used. The complete description of the model is shown by [99]. The wetting and drying scheme for the domain is implemented in the model, with a minimum water depth established to avoid negative values [102-103].

To calibrate and validate the model in order to study the transport of sediment in the Deep Navigation Channel DNC of the YRE, field data measured in 2009 were used. The data were collected after the construction of the two dikes and 19 groins; however, the water depth was about 10.5 m at that time [43-44]. The equation used in the model, the initial conditions for the hydrodynamics, and initial sediment distribution are all described in [44]. The physical and numerical parameters are summarized in table 2.

Parameter	Description	Value
w_{s50}	free settling velocity	$-1.715\times10^{-5}(ms^{-1})$
m_1	empirical settling coefficient	-0.014
n_1	empirical settling coefficient	2.20
m_2	empirical settling coefficient	2.89
n_2	empirical settling coefficient	2.80
C_0	Flocculate empirical coefficient	0.20 (kgm^{-3})
α	empirical coefficient	10.0
β	empirical coefficient	0.5
E_0	empirical erosion coefficient	$2.0\times10^{-5}(kgm^{-2}s^{-1})$
τ_c	critical shear stress for erosion or deposition	$0.05(kgm^{-1}s^{-2})$

Table 2. Parameters used in the sediment transport model [source: 44].

Tidal harmonic components from 8 sites were used to verify the model, and the root mean square error (RMSE). The tidal components used in the model were observed to represent nearly 95% of the tidal oscillation (i.e. M_2, S_2, K_1 and O_1). Tidal currents were used to verify the water speed, and a good agreement was achieved. Salinity measurements were used to verify the proper simulation of mixing in the YRE, and aside from the periods of highly vertical stratification during ebb currents, the model properly simulated the temporal variation in salinity at the sampling sites. The final validation of the model was to verify the proper simulation of the transport of SSC, and in general the model could reproduce the physical mechanism driving the transport of sediment well. In summary, aside from drawbacks such as over-mixing of salinity during the neap tide due to the 2.5 Mellor-Yamada turbulence closure scheme, the model was calibrated and verified, and thus was still a valuable tool to study and understand the influence the navigation channel has on the transport of sediment within YRE.

3.4. Setting up of the numerical model for the Darwin Harbour

To simulate the hydrodynamics and transport of sediment for Darwin Harbour, the unstructured numerical model FVCOM was applied [104]. The mesh was formed by 9,666 horizontal grid cells, and 20 vertical layers using sigma coordinate. The horizontal resolution varied between ~ 20 to ~3,300 m, with the higher resolution areas in the inner harbour and lower resolution in the outer harbour [76].

To force the model at the external open boundary, tidal forcing was used in the coastal area between Charles Point and Lee Point. The tidal components were obtained from TPXO7.2 global model. The semi-diurnal components used to force the model were (M_2, S_2, N_2 and K_2), while the diurnal components were (K_1, O_1, P_1 and Q_1). Three shallow-water components (M_4, MS_4, MN_4) and two extra tidal components of low frequency were also used, i.e.

M_f and M_m. For the internal boundary, e.g. upstream river zones, there are three sources of fresh water in the domain (Elizabeth River, Blackmore River and Berry Creek); however, the simulation was for the dry season and thus river discharge was negligible [76]. In the dry season, the small presence of density-driven currents is often confined upstream of Darwin Harbour, and they are often less than 3% of the maximum tidal current intensity. At the surface, the wind is an important mechanism to cause sediment resuspension, by wind-driven currents and waves [105]. The macro-tides in Darwin Harbour (typical tidal oscillation between 3.7 and 7.8 m), however, dominate the transport of sediment with tidal currents of up to ~ 3m s^{-1} [106]. The additional effects from wind, river discharge and the heat flux at the free-surface boundary were negligible, allowing the simulation to be forced by tides alone.

The bottom drag coefficient (C_d) was set to be a function of the water depth (see Eq. 2 in 76). The mangrove area was treated differently, because the influence of roots and trees significantly increase the friction and thus reduce water speed [107]. From empirical experiments C_d was observed to vary between 1 and 10, and its value relies upon tidal conditions, mangrove species, and patchiness of mangrove distribution. Therefore, the main value for C_d was set to 5. The remaining numerical and physical parameters, such as the viscosity and diffusion coefficient, are all described in more detail in [76].

For the initial conditions, constant values for salinity (33 psu) and temperature (25°C) were used. These are characteristic values during the dry season, and, with the zero river input, result in a barotropic model. The simulation started on 20th of June 2006 (00:00:00), with a one second time step, and duration of 31 days. Six different simulations were analysed, different sizes of tidal flats and mangrove areas were assumed, and one simulation excluding the presence of tidal flats and mangrove areas. These simulations provide an understanding of the independent effects of tidal flats and mangroves in the tidal asymmetry of Darwin Harbour. There were three main numerical experiments, namely: (Exp. 1) where tidal flats and mangrove areas were considered, (Exp. 2) where mangrove areas were removed from the domain, and (Exp. 3) where both mangrove and tidal flat areas were removed from the domain.

4. Results and discussion

4.1. Sediment transport in the Adriatic Sea

The key results from [84] are summarized as follows:

The Bora wind generated barotropic southward longshore currents that connected to the partially buoyancy driven WACC. This resulted in surface water currents of up to 1.3 m s^{-1} near the Po River mouth, and maximum bottom currents of 0.3 m s^{-1} near Ortona. These general features were all in concordance with [108]. The smooth wind conditions resulted in a reduced interior vorticity, which is caused by the orographic incisions around the Dinaric Alps [109]; however, the good representation of the WACC in the Nothern Adriatic Shelf combined with the wave-currents provided a realistic physical representation of sediment

http://dx.doi.org/10.5772/51022

transport during the Bora event. The Bora wind caused higher wave heights on the western coast than on the eastern coast. The wave direction was mainly aligned with the wind direction in the Adriatic Sea; however, the direction was mainly perpendicular when approaching the western coast because of wave refraction.

For low and moderate wind conditions, the modelled waves showed good agreement with observed waves. The measurements used to verify the model were obtained at the buoys at Ancona and Ortona. During strong wind conditions, such as Bora events, the model showed good results compared to observations of the waves at Ortona, while for Ancona the wave response was underestimated by 50%. This was caused by the low horizontal scale resolution of 40 km ECMWF wind fields. Due to the complex orography, the model is incapable of resolving the fine wind variability [91, 110].

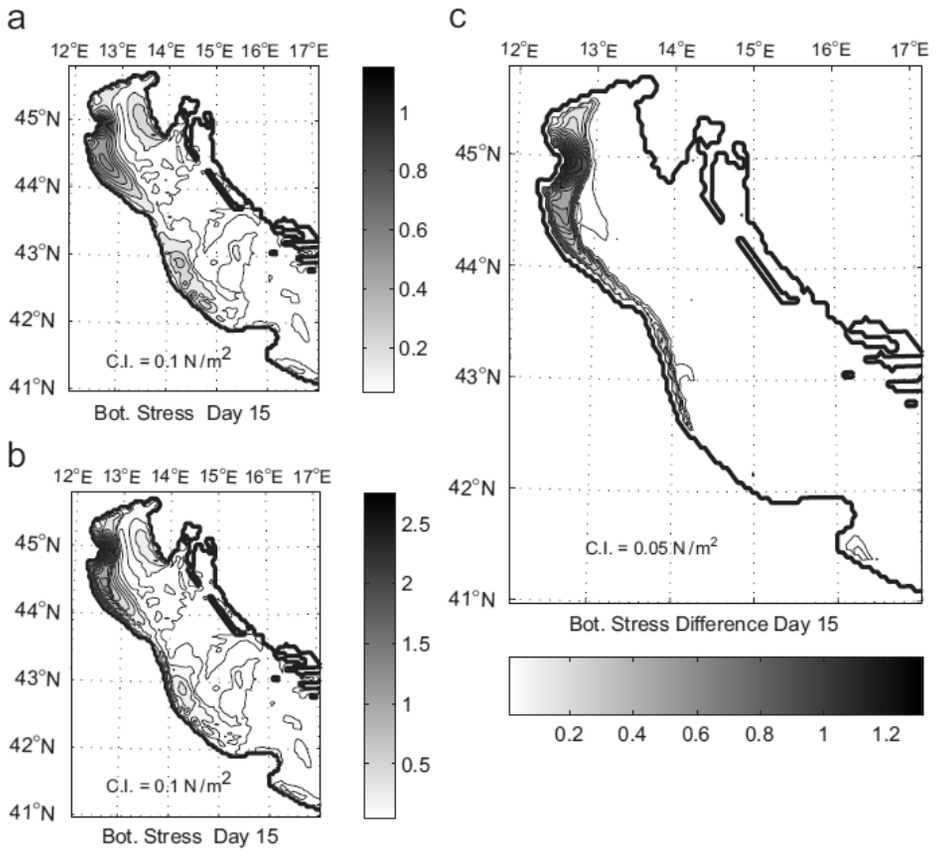

Figure 6. The bottom stress on 15 January 2001, predicted by Experiment 1 (a), Experiment 2 (b), and their difference (c) [source: 84].

Waves and currents have been shown to affect sediment resuspension in the Bottom Boundary Layer (BBL). Recent field studies conducted near the Po River delta were used to analyse the effect of wave-current interaction [e.g., 111-113]. The simulation without the wave effect (experiment 1) showed the bottom current reaching ~ 0.34 m s^{-1} during the Bora event. The Bora event caused the bottom stress to increase from 0.01 N m^{-2} to 0.66 N m^{-2} (Fig. 6a).

This increased bottom stress results in considerable erosion, and a subsequent increase in concentration of both fine and course sediment near the bottom. During periods without Bora winds, the resuspension was weak, and the fine sediment from the Po River discharge dominated the SSC in the water column. For experiment 2, in which the effect of wave-current interaction was considered (Fig. 6b), the bottom stress reached a maximum value of 2.2 N m^{-2}, and the concentration of fine and coarse sediments increased by 80%. (Fig. 7b). The wave-current interaction increased the bottom drag coefficient from 0.0048 to values of up to 0.015 (not shown).

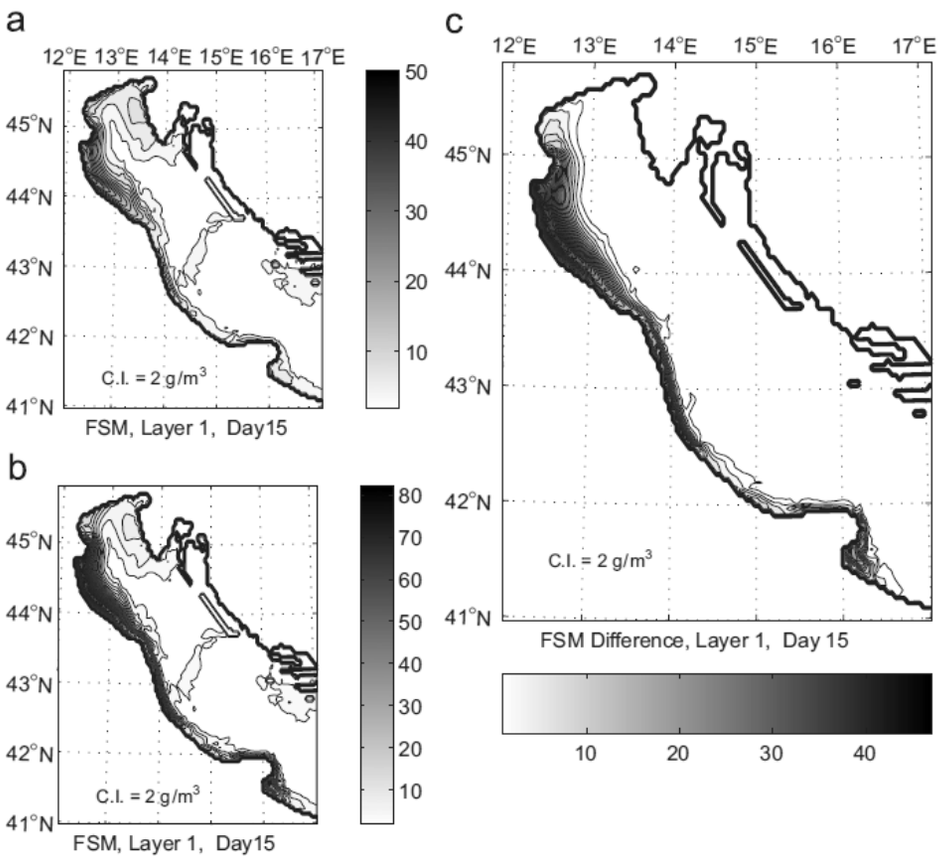

Figure 7. The surface (layer 1) fine sediment concentration on 15 January 2001, predicted by experiment 1 (a), Experiment 2 (b), and their difference (c) [source: 84].

In experiment 1, a high bottom stress was predicted in the north-east shelf along the Italian coast. Therefore, high SSC was obtained (i.e. 28 g m^{-3}) near the Po River delta, with similar concentration of coarse and fine sediments, which were very well vertically mixed. In experiment 2 the distribution patterns were very similar to those of experiment 1. The bottom stress and sediment concentration increased in magnitudes to 1.3 N m^{-2} and 50 g m^{-3}, respectively. This increase was verified along the coast (~ 200 km long), southwards from the Po River nearshore zone. It was observed that the prediction of the fine suspended sediment concentration showed good agreement with [112]. [113] has also obtained SSC in the range of 70-100 g m^{-3}.

http://dx.doi.org/10.5772/51022

The sediment flux was analysed in experiment 1, using results from a cross-sectional area. During the Bora event on 15th of January, an upwelling net sediment flux was observed, despite the downwelling currents along the Italian coast. The horizontal fields near the surface and bottom were also analysed, and a net sediment flux with maximum values of 20 g m^{-2} s^{-1}, was observed southwards near the Italian coast. The predictions were in agreement with estimates by [113] in a different Bora event. In experiment 1, the southward flux of 10.5 t s^{-1} (fine sediment) and 9.3 t s^{-1} (coarse sediment) was calculated at a cross-section area (N) near the Po River delta in the Adriatic Sea. In contrast, for experiment 2, the flux of fine and coarse sediment increased to 25.6 t s^{-1} and 24.1 t s^{-1}, respectively.

Experiment 3 was conducted to verify the effect from the wave and current aligned to the sediment transport. The net sediment flux of fine and coarse sediment was over predicted by 8% and 9%, respectively, from experiment 2. These small differences are evidence that the wave propagation direction had little effect on sediment flux. This was shown for strong wave conditions by [114].

To observe the effect of the tides, experiment 4 was conducted. It considered the same conditions as experiment 2, with the additional influence of tidal currents. The four main semi-diurnal tidal components were used (i.e. M_2, K_2, N_2, S_2), and the three main diurnal components (i.e. K_1, O_1, P_1). The sediment flux at the cross-sectional area (N) was observed to be reduced by 1%, compared with results from experiment 2.

The final experiment was similar to experiment 2. It included, however, the additional influence of sediment concentration on water density, using a simple bulk relation from [83]. Because of the small SSC, the effect on sediment flux was negligible, with slight changes of less than 1%.

4.2. Factors driving the phytoplankton bloom in the Mokpo coastal zone

The results showed little change in phytoplankton biomass throughout the entire water column during January. In contrast, in February the concentration of phytoplankton biomass increased at the surface. In the first two weeks of March this biomass increased significantly, and reached maximum values at the surface after two weeks (i.e. mid March). The model simulated the timing of the phytoplankton blooms well; however, the maximum biomass obtained from the theoretical results was 2-3 times lower than observed values. Some possible explanations for this underestimation are the short period of simulation (4 months), and the use of a 1-D biogeochemical model instead of a 3D model. Moreover, when the sluice gates located upstream are opened, the system temporally becomes a salt-wedge estuary. This increased fresh water input may cause the sinking riverine phytoplankton detritus that flows along the bottom. Additionally, there is a likely effect from the resuspended phytoplankton and/or detritus that were not incorporated in the model [33].

A good correlation was found between the variation in phytoplankton biomass and diatom concentrations. Despite the observed increase in radiance Q (W m^{-2}), the diatom bloom finished in April. Diatom concentration decreases mostly because of lack of dissolved phosphate (P) and silicate (Si) in the euphotic zone. This depletion is caused by phytoplankton

uptake combined with stratification-induced limitation of nutrient supply near the bottom. It has been shown that phytoplankton blooms develop due to a decrease in vertical mixing rates. Therefore, the increased vertical mixing that occurs from early January to mid-February inhibits the permanence of phytoplankton cells in the euphotic area [33]. Vertical mixing was increased due to the colder wind decreasing surface water temperatures, which then caused convective overturn in the water column.

The features of phytoplankton biomass (PB) variation were examined for light attenuation coefficients (Fc) of 0.43, 0.46 and 0.49 (Fig. 8). The PB over the euphotic zone increased slowly. All the blooms started at the same time, reaching nearly the same maximum of PB, i.e. 35 mg m^{-2}. However, the rates of increase were different, with maximum growth rate verified to occur for Fc = 0.49. Moreover, variation between neap and spring tides has also been shown to affect the PB. Water turbidity is increased due to larger sediment resuspension caused by the strong spring tidal current, and thus the PAR attenuation may affect phytoplankton production. The model results showed that the absence of the effect from SSC reduces PAR attenuation, and therefore changes phytoplankton production (not shown). Vertical mixing also affects the PB, because phytoplankton cells are taken to deeper layers where light attenuation is higher [33]. [115] proposed that blooms happen when phytoplankton growth exceeds the rate of vertical movement. Therefore, a decrease in vertical mixing results in phytoplankton blooms in coastal and oceanic waters [e.g. 116-118].

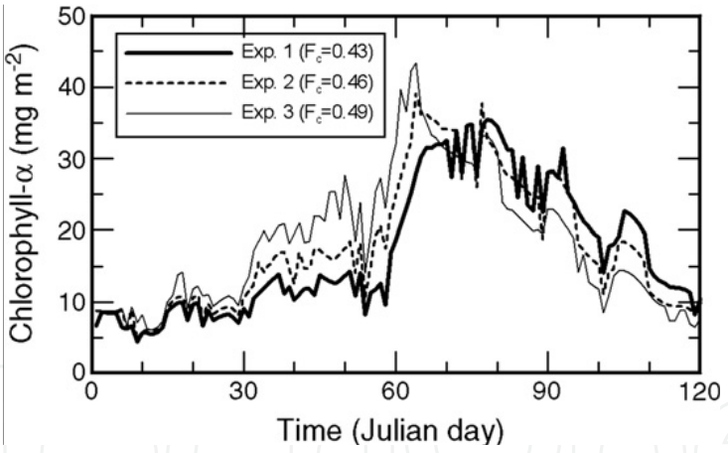

Figure 8. Temporal variation of the vertical integrated chlorophyll-a concentration in the euphotic zone. The numerical experiment for different values of Fc and the simulation start time at January 2001 [source: 33].

4.3. The effect of dikes on sediment transport in the Yangtze River Estuary

Tidal harmonic components were calculated using measurements from 8 water level stations, and later compared with results of the model. The root mean square error obtained for the 4 main components was under 10%, and the shift of tidal phases less than 10 degrees. In general, the model showed reasonable agreement compared with measurements of tidal oscillation, water current, and temporal variation of salinity and SSC. Details of the model calibration and verification are shown in [44]. The results of the SSC calculated from the model are shown in

http://dx.doi.org/10.5772/51022

(Fig. 9a). Differences between simulations and observations of the speed increase of the surface flood currents, during the rising sea level, were verified. Observations showed more steepness during flood tides, and, for a short period of time, measured flood current was approximately 20% higher than the model result. In contrast, water currents near the bottom consistently showed good agreement between modelled and observed values at any given time. Even with the minor differences found, the model was properly calibrated, and thus shown to be a valuable tool for studying sediment transport mechanisms in the YRE [44].

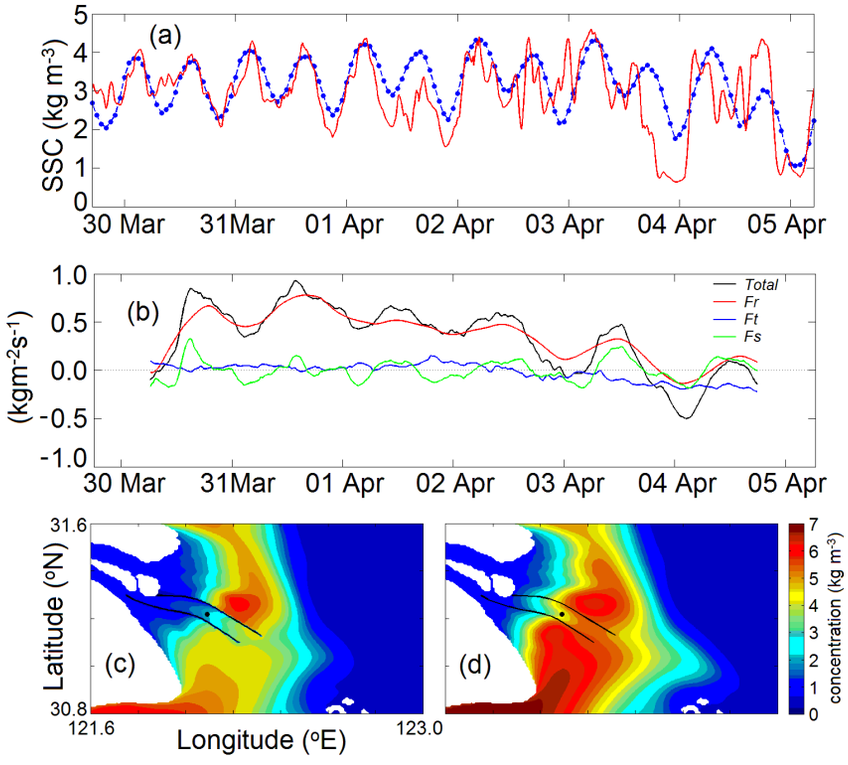

Figure 9. (a) Measured (red line) and model simulated (blue dotted line) suspended sediment concentration at 62 cm above the seabed. (b) The tidally averaged residual suspended sediment flux and its three components, i.e. residual flow (*Fr*), tidal pumping (*Ft*), and shear dispersion (*Fs*), where the positive value indicates ebb transport of SSC. (c) and (d) show the tidally averaged suspended sediment concentration after and before the DNC construction, respectively. The location of the dikes is indicated in both figures (c and d), and the location of the sampling station in the DNC (black dot).

Figure 9b shows field data results of the sediment transport near the bottom. During the spring tides between 30th of March and 2nd of April, there was more suspended sediment present at the onset of the ebb tide than at the onset of the flood tide. This resulted in a residual and tidal pumping transport of sediment downstream, where residual transport dominated the total transport of suspended sediment (TSS). Commonly, high residual TSS causes a downstream shear dispersion TSS, whereas low residual transport causes an upstream shear dispersion transport. In contrast, during the neap tide observed from the 2nd of April onwards, the bottom horizontal water velocities were much smaller than those observed during spring tides. Because of this, sediment resuspension decreased considerably, and

therefore the residual transport of SSC was reduced. In addition, tidal pumping was observed to transport SSC mainly landward. The residual transport and shear dispersion were observed to alternate SSC transport between upstream and downstream directions.

The results showed that the maximum SSC is generated in the sand bar area (Figs. 9c,d). The simulation in which the effect of the two dikes was applied (Fig. 9c) showed a discontinuity in the high SSC caused by the DNC, and the maximum SSC was observed adjacent to the north dike (e.g. SSC ~ 6 kg m^{-3}). In contrast, the simulation without the presence of dikes showed high SSC within the entire sand bar area near the estuarine mouth. The SSC decreasing upstream indicated a low local resuspension of sediment and a low sediment input from river discharge. In addition, the Three Gorges Dam caused a significant decrease in sediment load to the Yangtze River [60-61]. This local sediment resuspension is therefore evidence that the silting occurring within the DNC is caused by redistribution of sediment between the shoals on each side of the dikes.

Comparison between the simulations with and without the dikes, found enhanced ebb dominance to occur with the inclusion of the dikes (not shown). These changes have previously been observed and reported [63], by comparing field measurements obtained before and after construction of the dikes. After construction, the traditional sediment transport path across the estuarine mouth was blocked; however, some sediment may still be transported around the dike edges, and a small amount may enter the channel. This sediment intruding into the DNC is likely to cause siltation near the seaward side of the DNC.

4.4. Tidal asymmetry in Darwin Harbour

The amplitude of the M_2 tidal component was observed to gradually increase from the open boundary (i.e. outer harbour) to nearly 1.7 m in the arms, and decrease from the arms to nearly 1.0 and 0 meters in the tidal flat and mangrove areas, respectively. The decrease in amplitude for the tidal flat and mangrove areas was caused by large energy dissipation due to bottom friction. The phase shifted in areas of the outer harbour and harbour arms, and this shift was caused by reduced wetting-drying areas. The maximum horizontal velocity is about 3.0 m s^{-1} in the Middle Arm (see Fig. 5). The variation of M_2 tidal current ellipses were observed at many vertical layers and locations of the domain. In the outer harbour the M_2 currents were up to 0.3 m s^{-1}, and up to 0.6 m s^{-1} in the channel. The horizontal currents were observed to decrease by almost 30 % from the surface to the bottom [76].

Comparison of the three numerical experiments from simulations that neglected the tidal flat or mangrove areas, showed an increase in the tidal amplitude for the inner and outer harbour. The maximum increase was obtained when both tidal flats and mangroves areas were not considered in the domain (0.02 m), while there was an increase of 0.01 m for the simulation neglecting only the mangrove areas. Although the variation of tidal amplitude was observed to be quite small, for the M_4 tidal component, there was an increase in amplification of almost 50% when the mangrove areas were removed, and almost 75% when both the tidal flats and mangrove areas were removed. The phase of the M_4 tidal component was observed to advance almost 20 degrees when the mangrove areas and tidal flats were not included in the domain [76].

http://dx.doi.org/10.5772/51022

To verify the effect of mangrove and tidal flat areas on tidal asymmetry, the tidal asymmetry skewness parameter γ was calculated. This allows identification of the major factors controlling tidal asymmetry. For γ, it was verified that the main tidal components controlling tidal asymmetry were M_2 and M_4, and so the expression to calculate γ was:

$$\gamma_{M_2/M_4} = \frac{\frac{3}{2} a_{M_2}^2 a_{M_4}^2 \sin\left(2\phi_{M_2} - \phi_{M_4}\right)}{\left[\frac{1}{2}\left(a_{M_2}^2 + 4a_{M_4}^2\right)\right]^{\frac{3}{2}}} \quad (1)$$

where a and ϕ are respectively the amplitudes, and phases of the astronomical tides M_2 and M_4.

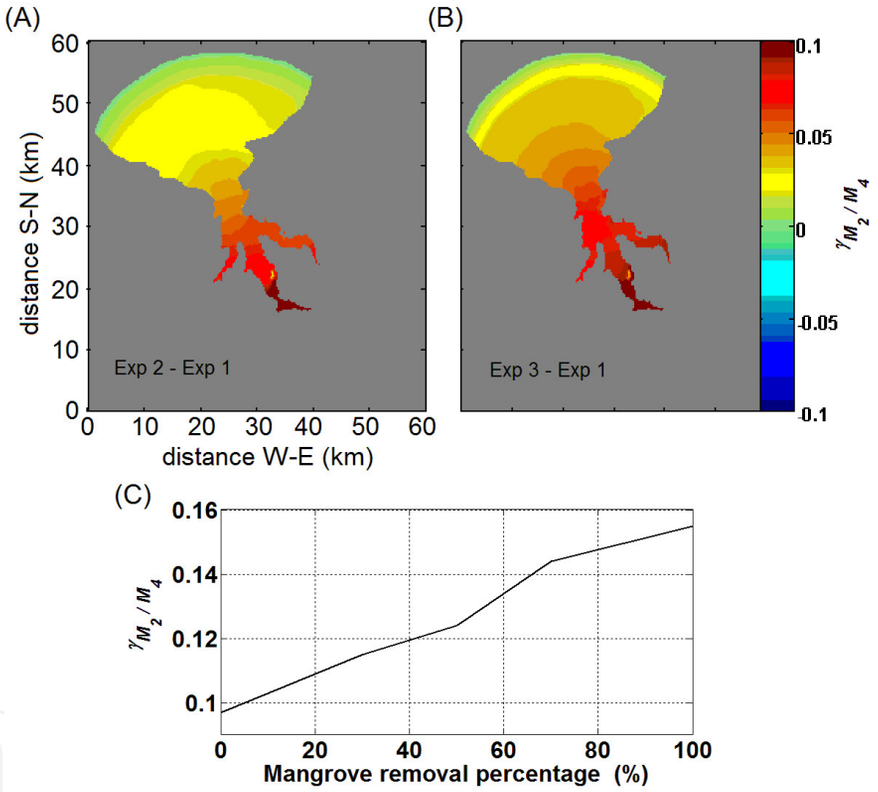

Figure 10. Predicted changes of the coefficient (γ), with results obtained from the difference between experiment 2 and 1 (A), and 3 and 1 (B). (C) Parameter γ calculated for different percentages of mangrove area removed in the East Arm near Station Blay [source: 76].

Figure 10 shows that the removal of mangroves and tidal flat areas resulted in an increased tidal asymmetry. In turn, Darwin Harbour would have more flood dominance in tidal currents (Figs. 10A,B). The maximum increase in asymmetry was observed in experiment 3. The experiments in which different percentages of the mangrove areas were removed are shown in figure 10C. The relation between removed mangrove area and increased tidal asymmetry skewness factor was observed to be almost linear, and increased by 0.1 if 100% of the man-

grove areas were removed. These results demonstrate that the tidal flats and mangrove zones function as sponge zones for dampening tidal asymmetry [76].

5. Conclusions

This chapter provided information about four important suspended sediment transport processes. It showed how wave current interaction increases SSC and therefore affects the net transport of sediment, and demonstrated the importance of applying a coupled hydrodynamical and biogeochemical numerical model to better simulate phytoplankton blooms. In addition, the effect of coastal construction on sediment transport was described, along with the role of tidal flats and mangrove areas in causing tidal asymmetry. Specific conclusions for each case study are as follows:

5.1. Effect of wave current interaction on sediment transport in coastal zones

The general features of the model during the Bora event in January 2001 predicted the WACC, and the large wave fields generated by the strong winds agreed with observations on the western Adriatic shelf. The bottom boundary layer was resolved, and the wave-current interaction was able to be implemented in the model. Moreover, the tidal effect on sediment transport was also examined in the Northern Adriatic Sea.

The model showed that the Bora event occurring from 13–17 January 2001 caused waves with height of 2 m, and period of 5 s. The wave-current near the bottom layer resulted in strong sediment resuspension. The wave effect, combined with the longshore coastal currents and the turbulent driven vertical flux, caused a large southward sediment flux. The flux was estimated using data from a cross-section area of the Adriatic Sea, near the Po River. The experiment including the wave-current interaction showed larger southward sediment flux than the experiment with waves neglected. The sediment flux was clearly maintained by the strong vertical mixing and the bottom sediment resuspension. The results also showed that the southward flux was more confined to the northern area of the Adriatic Sea, and sediment plumes were confined to the western Adriatic shelf north of Ancona.

Simulation results have shown that in areas between the Po River and Ancona, sedimentation and erosion rates doubled due to the combined motion of wave–current interaction in the BBL during the Bora event. Bora events typically occur 9 times during winter seasons [119], and thus the influence of waves is important in the long-term sediment transport at this coastal area. The annual sedimentation rate near the Po River mouths was found to be 2-6 cm yr^{-1} [120]. The sedimentation rate predicated during the Bora event of 13-17 January 2001 represented nearly 10% of the annual rate. This prediction agrees with observations if we assume the average of ~ 10 Bora events per year. In addition, from experiment 2, it was verified that the high concentration of suspended sediment along the western coast, north of Ancona, was locally driven by waves. Moreover, the wave-current interaction with the BBL enhanced the bottom stress and caused increased sediment resuspension. From the third ex-

http://dx.doi.org/10.5772/51022

periment it was observed at the cross-sectional area (N), that wave direction and tides had little effect on sediment resuspension in the northeastern coast of the Adriatic Sea.

5.2. Effect of SSC on phytoplankton bloom

Simulation of phytoplankton biomass dynamics was obtained during the winter and spring seasons. The model was run using irradiance forcings and physical oceanographic forcings such as SSC, temperature, salinity, tides, and vertical diffusivity. The results from winter revealed that cooling of the surface waters induced vertical mixing, and thus inhibited the growth of phytoplankton biomass. In contrast, periods of neap tides combined with increased freshwater discharge decreased vertical mixing, and in turn triggered PB spring bloom. In the tidally turbid coastal waters, such as the MCZ, the small neap tidal currents were not capable of increasing SSC. As a result, more light was observed though the water column, favouring increases in phytoplankton biomass [33].

Results revealed that prediction of phytoplankton blooms are very sensitive to the light attenuation factor (Fc), vertical diffusion (*Kv),* and suspended sediment concentration (SSC). Moreover, simulations using depth-averaged diffusivity and monthly averaged vertical diffusivity, may hinder the primary production processes. Finally, the simulations revealed the importance of coupling the 3D hydro-sediment model with the ecosystem model, which leads to more realistic estimates of phytoplankton biomass oscillation [33].

5.3. Influence of coastal construction on sediment transport

The simulations were well calibrated and validated using field data measured in the DNC in Shanghai Port on March 2009. Combining the field measurements with the extrapolated results for the whole domain of the YRE, we have verified that the system is highly stratified during neap tides; however, close to well mixed during spring tides. Calculation of the Richardson number revealed the dominance of fresh water inflow over vertical mixing during neap tides; while, in spring tides, vertical mixing overcomes the buoyancy of the fresh water river inflow [44].

The simulations revealed that the transport of sediment into the DNC comes from open areas, rather than from upstream areas as is commonly expected. Therefore, the input from the Yangtze River is not the major source of sediment, causing siltation, in this navigation channel. The dikes were observed to inhibit the majority of the alongshore sediment transport near the delta zone; however some of the sediment transported towards the dikes veers south, and as it approaches the edges of the dikes a small amount may enter the channel. It was verified that, in the North Channel, the estuarine maximum turbidity zone was generated predominantly by gravitational circulation, whereas, in the South Passage, it was generated mainly by tidal distortion effects. For the DNC there was no maximum turbidity generated locally. Some turbid waters in adjacent areas were observed to be transported upstream in this channel. In summary, the simulation results revealed the magnitude of the maximum turbidity zone in the North Passage, and showed that most of the sediment depositing into the DNC is caused by sediment redistribution from adjacent zones [44].

5.4. Tidal asymmetry modulated by tidal flats and mangrove areas

The results obtained from the simulations, combined with field observations, showed that the circulation in DH is mainly driven by tides during the dry season, with negligible wind and river influence. DH is a semidiurnal system, dominated primarily by the M_2 tidal component, and secondarily by the S_2 component. The maximum velocities observed were in the Middle Arm, with peaks of over 3.0 m s^{-1} at the surface layer. The Middle Arm also had the maximum and minimum vertical shear of the horizontal velocities, which would therefore result in some of the maximum vertical mixing zones of DH.

The sensitivity test evidenced that tidal flats and mangrove areas play an important role in modulating the amplitude and phase of some tidal components. In particular, the amplitude of the M_4 component was observed to increase by almost 75%, and the phase was verified to advance/delay a few degrees in the outer/inner harbour respectively. In addition, the amplitude and phase of the M_2 component were observed to change in the inner harbour, with an amplitude increase of 1% and phase advance of 4 degrees.

The parameter gamma was calculated, showing variation in the tidal elevation skewness. Gamma was observed to increase by 100% in the absence of mangrove areas, and by 120% in the absence of both tidal flats and mangrove areas. Furthermore, the increase in the elevation skewness correlated almost linearly with the decrease in mangrove area. It was therefore suggested that a similar effect would be found with a decrease in tidal flat areas. The findings of this study show how important flooding estuarine areas, e.g. tidal flats and mangroves, are in modulating tidal asymmetry. These findings could be further used to verify similar effect in other estuaries, bays, and harbour areas. As tidal asymmetry strongly affects sediment transport in the estuaries, care must be taken in terms of the reclamation of the mangrove areas and tidal flats around the harbour watershed.

Acknowledgements

X. H. Wang and F. P. Andutta were supported by a 2011 Australian Research Council/ Linkage Project – LP110100652. This work was also supported by the National Computational Infrastructure National Facility at the Australian National University. This is a publication of the Sino-Australian Research Centre for Coastal Management, paper number 10.

Author details

X. H. Wang* and F. P. Andutta

*Address all correspondence to: hua.wang@adfa.edu.au

School of Physical, Environmental and Mathematical Sciences, University of New South Wales at Australian Defence Force Academy UNSW-ADFA, Australia

http://dx.doi.org/10.5772/51022

References

[1] Wang, X. H., & Pinardi, N. (2002). Modeling the dynamics of sediment transport and resuspension in the northern Adriatic Sea. *Journal of Geophysical Research*, 107(C12), 3225, doi:10.1029/2001JC001303.

[2] Frascari, F., Frignani, M., Guerzoni, S., & Ravaioli, M. (1988). Sediments and pollution in the Northern Adriatic Sea. *Annals of the New York Academy Sciences*, 534, 1000-1020.

[3] Giordani, P., Hammond, D. E., Berelson, W. M., Montanari, G., Poletti, R., Milandri, A., Frignani, M., Langone, L., Ravailoi, M., Rovatti, G., & Rabbi, E. (1992). Benthic fluxes and nutrient budgets for sediments in the Northern Adriatic Sea: Burial and recycling efficiencies. *Science of the Total Environment, Supplement*, 251-275.

[4] Wolanski, E. (2007). *Estuarine Ecohydrology*, Elsevier, Amsterdam, 157.

[5] Warren, R., & Johnsen, J. (1993, June 14-16, 1993). Cohesive sediment modelling for coastal lagoons. Kuala Lumper, Malaysia. *paper presented at International Colloquium and Exposition on Computer Applications in Coastal and Offshore Engineering (ICE-CA COE'93)*.

[6] Vichi, M., Pinardi, N., Zavatarelli, M., Matteucci, G., Marcaccio, M., Bergamini, M. C., & Frascari, F. (1998). One-dimensional ecosystem model tests in the Po Prodelta area (Northern Adriatic Sea). *Environmental Modelling & Software*, 13, 471-481.

[7] Wolanski, E., Andutta, F. P., & Delhez, E. (2012). Estuarine hydrology. *In: Encyclopedia of Lakes and Reservoirs. Lars Bengtsson, Reginald Herschy, Rhodes Fairbridge (eds.)*, Springer, In press.

[8] Maggi, F. (2005). Flocculation dynamics of cohesive sediment. *PhD-Thesis*, Delft University of Technology, Delft, 136.

[9] Kourafalou, V. H. (1999). Process studies on the Po River plume, North Adriatic Sea. *Journal of Geophysical Research*, 104, 29963-29985.

[10] Wang, X. H. (2005). A numerical study of sediment transport in a coastal embayment during a winter storm. *Ocean Modelling*, 10, 253-271.

[11] Milliman, J. D., & Farnsworth, K. L. (2011). *River Discharge to the Coastal Ocean: A Global Synthesis*, Cambridge University Press, 392.

[12] Vilibić, I. (2003). An analysis of dense water production on the North Adriatic shelf. *Estuarine, Coastal and Shelf Science*, 56, 697-707.

[13] Malanotte-Rizzoli, P., & Bergamasco, A. (1983). The dynamics of the coastal regions of the Northern Adriatic Sea. *Journal of Physical Oceanography*, 13, 1105-1130.

[14] Artegiani, A., Bregant, D., Paschini, E., Pinardi, N., Raicich, F., & Russo, A. (1997a). The Adriatic Sea general circulation. Part I: air-sea interactions and water mass structure. *Journal of Physical Oceanography*, 27, 1492-1514.

[15] Artegiani, A., Bregant, D., Paschini, E., Pinardi, N., Raicich, F., & Russo, A. (1997b). The Adriatic Sea general circulation. Part II: Baroclinic circulation structure. *Journal of Physical Oceanography*, 27, 1515-1532.

[16] Zavatarelli, Z., Pinardi, N., Kourafalou, V. H., & Maggiore, A. (2002). Diagnostic and prognostic model studies of the Adriatic Sea general circulation: Seasonal variability. *Journal of Geophysical Research*, 107, 3004, doi:10.1029/2000JC000210.

[17] Zavatarelli, M., & Pinardi, N. (2003). The Adriatic Sea modelling system: a nested approach. *Annales Geophysicae*, 21, 345-364.

[18] Poulain, P. M. (2001). Adriatic Sea surface circulation as derived from drifter data between 1990 and 1999. *Journal of Marine System*, 29, 3-32.

[19] Raicich, F. (1996). On the fresh water balance of the Adriatic Sea. *Journal of Marine System*, 9, 305-319.

[20] Haley, J. P. J., & Lermusiaux, P. F. J. (2010). Multiscale two-way embedding schemes for free-surface primitive equations in the "Multidisciplinary simulation, estimation and assimilation system". *Ocean Dynamics*, 60, 1497-1537.

[21] Ramp, S. R., Lermusiaux, P. F. J., Shulman, I., Chao, Y., Wolf, R. E., & Bahr, F. L. (2011). Oceanographic and atmospheric conditions on the continental shelf north of the Monterey Bay during August 2006. *Dynamics of Atmospheres and Oceans*, 52, 192-223.

[22] Andutta, F. P., Ridd, P. V., & Wolanski, E. (submitted). *Age and the flushing time in the Great Barrier Reef coastal waters*.

[23] Nunes, Vaz. R. A., Lennon, G. W., & Bowers, D. G. (1990). Physical behaviour of a large, negative or inverse estuary. *Continental Shelf Research*, 10, 277-304.

[24] Diop, E. S., Soumare, A., Diallo, N., & Guisse, A. (1997). Recent change of mangroves of the Saloum river estuary, Senegal. *Mangroves and Salt Marshes*, 1, 163-172.

[25] Largier, J. L., Hollibaugh, J. T., & Smith, S. V. (1997). Seasonally hypersaline estuaries in Mediterranean-climate regions. *Estuarine, Coastal and Shelf Science*, 45, 789-797.

[26] Lavin, M. F., Godinez, V. M., & Alvarez, L. G. (1998). Inverse-estuarine features of the upper gulf of California. *Estuarine, Coastal and Shelf Science*, 47, 769-795.

[27] Webster, I. T. (2010). The hydrodynamics and salinity regime of a coastal lagoon- The Coorong Australia- Seasonal to multi-decadal timescales. *Estuarine Coastal and Shelf Science*, 90, 264-274.

[28] Andutta, F. P., Ridd, P. V., & Wolanski, E. (2011). Dynamics of hypersaline coastal waters in the Great Barrier Reef. *Estuarine, Coastal and Shelf Sciences*, 94, 299-305.

[29] Winant, C. D., & de Velasco, G. G. (2012). Dynamics of hypersaline estuaries: Laguna San Ignacio, Mexico. Chapter 12 in, 2, *In: Uncles R J, Monismith S G (Ed.), Water and Fine Sediment Circulation. In: Wolanski E, McLusky D (Series Ed.), The Treatise on estuarine and coastal Science*, Elsevier.

[30] Nunes, Vaz. R. A. (2012). The salinity response of an inverse estuary to climate change & desalination. *Estuarine, Coastal and Shelf Sciences*, 98, 49-59.

[31] Brambati, A., Bregant, D., Lenardon, G., & Stolfa, D. (1973). Transport and sedimentation in the Adriatic Sea. *Museo Friulano di Storia Nat.*, Udine, Italy, Publ. 20, 60.

[32] Byun, D. S., Wang, X. H., & Holloway, P. E. (2004). Tidal characteristic adjustment due to dyke and seawall construction in the Mokpo Coastal Zone, Korea. *Estuarine, Coastal and Shelf Science*, 59, 185-196.

[33] Byun, D. S., Wang, X. H., Zavantarelli, M., & Cho, Y. K. (2007). Effects of resuspended sediments and vertical mixing on phytoplankton spring bloom dynamics in a tidal estuarine embayment. *Journal of Marine Systems*, 67, 102-118.

[34] Defant, A. (1960). *Physical Oceanography*, Pergamon Press, New York, 2, 598.

[35] Kang, J. W. (1999). Changes in tidal characteristics as a result of the construction of sea-dike/sea-walls in Mokpo coastal zone in Korea. *Estuarine, Coastal and Shelf Science*, 48, 429-438.

[36] Kang, J. W., & Jun, K. S. (2003). Flood and ebb dominance in estuaries in Korea. *Estuarine, Coastal and Shelf Science*, 56, 187-196.

[37] Kang, J. W., Moon, S. R., & Lee, K. H. (2009). Analyzing sea level rise and tide characteristics change driven by coastal construction at Mokpo Coastal Zone in Korea. *Ocean Engineering*, 36, 415.

[38] Speer, P. E., & Aubrey, D. G. (1985). A study of nonlinear tidal propagation in shallow inlet/estuarine systems. Part II: theory. *Estuarine, Coastal and Shelf Science*, 21, 207-224.

[39] Lee, S. W. (1994). Change in tidal height at Mokpo Harbour due to the construction of Youngsan River Estuary Dyke. *Korean harbour hydraulics*, 18, 27e37, in Korean.

[40] Jeong, M. S., Jeong, D. D., Shin, S. H., & Lee, J. W. (1997). Tidal changes in the harbor due to the development of Mokpo Coastal Zone. *Journal of Korean Harbour*, 11, 1e8, in Korean.

[41] Milliman, J. D., Shen, H., Yang, Z., & Meades, R. H. (1985). Transport and deposition of river sediment in the Changjiang estuary and adjacent continental shelf. *Continental Shelf Research*, 4(1/2), 37-45.

[42] Milliman, J. D., & Syvitski, J. P. M. (1992). Geomorphic/tectonic control of sediment discharge to the ocean: the importance of small mountainous rivers. *Journal of Geology*, 100(5), 525-544.

[43] Cao, Z., Wang, X. H., Guan, W., Hamilton, L. J., Chen, Q., & Zhu, D. (submitted). Observations of nepheloid layers in the Yangtze estuary, China. *Marine Technology Society Journal*.

[44] Song, D., & Wang, X. H. (inpreparation). *Observation and Modelling Study of the Turbidity Maximum in the Deepwater Navigation Channel in the Yangtze River Estuary*.

[45] He, Q., Li, J., Li, Y., Jin, X., & , Y. (2001). Field measurements of bottom boundary layer processes and sediment resuspension in the Changjiang estuary. *Science in China (Series B)*, 44(Supp.), 80-86.

[46] Shi, J. Z., Zhang, S. Y., & Hamilton, L. J. (2006). Bottom fine sediment boundary layer and transport processes at the mouth of the Changjiang Estuary, China. *Journal of Hydrology*, 327(1/2), 276-288.

[47] Liu, G., Zhu, J., Wang, Y., Wu, H., & Wu, J. (2011). Tripod measured residual currents and sediment flux Impacts on the silting of the Deepwater Navigation Channel in the Changjiang Estuary. *Estuarine, Coastal and Shelf Science*, 93(3), 192-201.

[48] Li, J., & Zhang, C. (1998). Sediment resuspension and implications for turbidity maximum in the Changjiang Estuary. *Marine Geology*, 148(3-4), 117-124.

[49] Shi, Z., & Kirby, R. (2003). Observations of fine suspended sediment processes in the turbidity maximum at the North Passage of the Chanjiang estuary, China. *Journal of Coastal Research*, 19(3), 529-540.

[50] Shi, Z. (2004). Behaviour of fine suspended sediment at the North passage of the Changjiang Estuary, China. *Journal of Hydrology*, 293(1-4), 180-190.

[51] Shen, H., & Pan, D. (2001). *Turbidity maximum in the Changjiang Estuary*, China Ocean Press, Beijing, in Chinese with English introduction, 194.

[52] Yang, Z., Milliman, J. D., & Fitzgerald, M. G. (1982). Transfer of Water and Sediment from the Yangtze River to the East China Sea, June 1980. *Canadian Journal of Fisheries and Aquatic Sciences*, 40(S1), 72-82.

[53] Milliman, J. D., Hsueh, Y., Hu, D., Pashinski, D. J., Shen, H., Yang, Z., & Hacker, P. (1984). Tidal phase control of sediment discharge from the Yangtze River. *Estuarine, Coastal and Shelf Science*, 19(1), 119-128.

[54] Beardsley, R. C., Limeburner, R., Yu, H., & Cannon, G. A. (1985). Discharge of the Changjiang (Yangtze River) into the East China Sea. *Continental Shelf Research*, 4(1-2), 57-76.

[55] Su, J., & Wang, K. (1986). The suspended sediment balance in Changjiang Estuary. *Estuarine Coastal and Shelf Science* , 23(1), 81-98.

[56] Shen, H., Li, J., Zhu, H., Han, M., & Zhou, F. (1993). Transport of the suspended sediment in the Changjiang Estuary. *International Journal of Sediment Research*, 7, 45-63.

[57] Shen, J., Shen, H., Pan, D., & Xiao, C. (1995). Analysis of transport mechanism of water and suspended sediment in the turbidity maximum of the Changjiang Estuary. *Acta Geographica Sinica*, 50(5), 411-420, in Chinese with English abstract.

[58] Hamilton, L. J., Shi, Z., & Zhang, S. Y. (1998). Acoustic backscatter measurements of estuarine suspended cohesive sediment concentration profiles. *Journal of Coastal Research*, 14(4), 1213-1224.

[59] Gao, J., Yang, Y., Wang, Y., Pan, S., & Zhang, R. (2008). Sediment dynamics of turbidity maximum in Changjiang River mouth in dry season. *Frontiers of Earth Science in China*, 2(3), 249-261.

[60] Chen, X., & Zong, Y. (1998). Coastal erosion along the Changjiang deltaic shoreline, China: History and prospective. *Estuarine Coastal and Shelf Science*, 46(5), 733-742.

[61] Yang, Z., Wang, H., Saito, Y., Milliman, J. D., Xu, K., Qiao, S., & Shi, G. (2006). Dam impacts on the Changjiang (Yangtze) River sediment discharge to the sea: The past 55 years and after the Three Gorges Dam. *Water Resource Research*, 42, W04407, doi: 10.1029/2005WR003970.

[62] Wu, H., & Guo, W. (2004). The physical model study on suspend sediment back silting in navigation channel of Yangtze River Estuary. *Shanghai Estuarine and Coastal Science Research Centre*, in Chinese.

[63] Tan, Z., Fan, Q., Zheng, W., & Zhu, J. (2011). Analysis of reasons for the siltation in North Passage of Yangtze Estuary. *Port & Waterway Engineering* [1], 29-40, in Chinese with English abstract.

[64] He, S., & Sun, J. (1996). Characteristics of suspended sediment transport in the turbidity maximum of the Changjiang River Estuary. *Oceanologia et Limnologia Sinica*, 27(1), 60-66, in Chinese with English abstract.

[65] Chen, J., Li, D., Chen, B., Hu, F., Zhu, H., & Liu, C. (1999). The processes of dynamic sedimentation in the Changjiang Estuary. *Journal of Sea Research*, 41(1-2), 129-140.

[66] Wu, J., Wang, Y., & Cheng, H. (2009). Bedforms and bed material transport pathways in the Changjiang (Yangtze) Estuary. *Geomorphology*, 175-184.

[67] Ge, J., Ding, P., & Chen, C. (2010). Impacts of Deep Waterway Project on local circulations and salinity in the Changjiang Estuary, China. Shanghai, China. *paper presented at the 32nd International Conference on Coastal Engineering*.

[68] Shi, J. Z. (2010). Tidal resuspension and transport processes of fine sediment within the river plume in the partially-mixed Changjiang River estuary, China. *A personal perspective Geomorphology*, 121(3-4), 133-151.

[69] Shi, J. Z., Zhou, H. Q., Liu, H., & Zhang, Y. G. (2010). Two-dimensional horizontal modeling of fine-sediment transport at the South Channel-North Passage of the partially mixed Changjiang River estuary. *China Environment Earth Sciences*, 61(8), 1691-1702.

[70] Wilson, D., Padovan, A., & Townsend, S. (2004). The Water Quality of Spring and Neap Tidal Cycles in the Middle Arm of Darwin Harbour during the Dry Season. *Water Monitoring Branch, Natural Resource Management Division*, Department of Infrastructure, Planning and Environment, Darwin.

[71] Brocklehurst, P., & Edmeades, B. (1996). The Mangrove Communities of Darwin Harbour. *Tech Memo.* [96].

[72] Tien, A. T. (2006). Influence of deep aquifer springs on dry season stream water quality in Darwin Rural Area. *Water Monitoring Branch Natural Resource Management Division Report*, 6/2006D, 54.

[73] Michie, M. G. (1987). Distribution of foraminifera in a macrotidal tropical estuary: Port Darwin, Northern Territory of Australia. *Australian Journal of Marine and Freshwater Research*, 38, 249-259.

[74] Woodroffe, C. D., Bardsley, K. N., Ward, P. J., & Hanley, J. R. (1988). Production of mangrove litter in a macrotidal embayment, Darwin Harbour, N.T., Australia. *Estuarine, Coastal and Shelf Science*, 26(6), 581-598.

[75] Li, L., Wang, X. H., Sidhu, H., & Williams, D. (2011). Modelling of three-dimensional tidal dynamics in Darwin Harbour, Australia. *in Proceedings of the 15th Biennial Computational Techniques and Applications Conference (CTAC-2010)*, 52, C103-C123.

[76] Li, L., Wang, X. H., Williams, D., Sidhu, H., & Song, D. (2012). Numerical study of the effects of mangrove areas and tidal flats on tides: A case of study of Darwin Harbour, Australia. *Journal of Geophysical Research*, In press.

[77] Padovan, A. V. (1997, December). The water quality of Darwin Harbour: October 1990 - November 1991. *Water Quality Branch, Water Resources Division, Department of Lands, Planning and Environment, NT Government, Report* [34/1997D].

[78] Williams, D., Wolanski, E., & Spagnol, S. (2006). Hydrodynamics of Darwin Harbour. *In: Wolanski E, editor. The Environment in Asia Pacific Harbours*, Springer, Printed in The Netherlands, 461-476.

[79] Williams, D. (2009). Part 1: hydrodynamics and sediment transport. *In Dredging of sand from Darwin Harbour, hydrographic and marine life, Australian Institute of Marine Science, Arafura Timor Research Facility*, Brinkin, Northern Territory, 1-33.

[80] Ribbe, J., & Holloway, P. E. (2001). A model of suspended sediment transport by internal tides. *Continental Shelf Research*, 21, 395-422.

[81] Wang, X. H. (2001). A numerical study of sediment transport in a coastal embayment during a winter storm. *Journal of Coastal Research*, 34, 414-427.

[82] Wang, X. H. (2002). Tide-induced sediment resuspension and the bottom boundary layer in an idealized estuary with a muddy bed. *Journal of Physical Oceanography*, 32, 3113-3131.

[83] Wang, X. H., Pinardi, N., & Malacic, V. (2007). Sediment transport and resuspension due to combined motion of wave and current in the northern Adriatic Sea during a Bora event in January 2001: A numerical modelling study. *Continental Shelf Research*, 27, 613-633.

[84] Blumberg, A. F., & Mellor, G. L. (1987). A description of a three-dimensional coastal ocean circulation model. *in Three dimensional Coastal Ocean Models, edited by N. S. Heaps*, American Geophysical Union, Washington D. C., 1-16.

[85] Smagorinsky, J. (1963). General circulation experiments with the primitive equations, I: the basic experiment. *Monthly Weather Review*, 91, 99-164.

[86] Nittrouer, C., Miserocchi, S., & Trincardi, F. (2004). The PASTA project: investigation of Po and Apenine sediment transport and accumulation. *Oceanography*, 17(4), 46-57.

[87] Adams, C. E., Jr , , & Weatherly, G. L. (1981). Some effects of suspended sediment stratification on an oceanic bottom boundary layer. *Journal of Geophysical Research*, 86, 4161-4172.

[88] Trowbridge, J. H., & Kineke, G. C. (1994). Structure and dynamics of fluid muds over the Amazon continental shelf. *Journal of Geophysical Research*, 99, 865-874.

[89] Fohrmann, H., Backhaus, J. O., Laume, F., & Rumohr, J. (1998). Sediments in bottom-arrested gravity plumes: numerical case studies. *Journal of Physical Oceanography*, 28, 2250-2274.

[90] Cavaleri, L., & Bertotti, L. (1997). In search of the correct wind and wave fields in a minor basin. *Monthly Weather Review*, 125, 1964-1975.

[91] Mellor, G. L., & Yamada, T. (1982). Development of a turbulence closure model for geophysical fluid problems. *Reviews of Geophysics and Space Physics*, 20(4), 851-875.

[92] Byun, D. S., & Wang, X. H. (2005). Numerical studies on the dynamics of tide and sediment transport in the western tip of the southwest coast, Korea. *Journal of Geophysical Research*, 110, C03011.

[93] Baretta, J. G., Ebenhöh, W., & Ruardij, P. (1995). The European regional seas ecosystem model, a complex marine ecosystem model. *Netherlands Journal of Sea Research*, 33, 233-246.

[94] Legendre, L., & Rassoulzadegan, F. (1995). Plankton and nutrient dynamics in marine waters. *Ophelia*, 41, 153-172.

[95] Vichi, M., Oddo, P., Zavatarelli, M., Coluccelli, A., Coppini, G., Celio, M., Fonda, Umani. S., & Pinardi, N. (2003). Calibration and validation of a one-dimensional complex marine biogeochemical fluxes model in different areas of the northern Adriatic Sea. *Annales Geophysicae*, 21(2), 413-437.

[96] Yoon, Y. H. (2000). On the distributional characteristics of phytoplankton community in Mokpo Coastal Waters, Southwestern Korea during low temperature season. *Journal of Institute for Basic Sciences*, Yosu Natinia University, 2, 71-82, in Korean.

[97] Blumberg, A. F., & Mellor, G. L. (1983). Diagnostic and prognostic numerical circulation studies of the South Atlantic Bight. *Journal of Geophysical Research*, 88(C8), 4579-4592.

[98] Mellor, G. L. (2004). Users guide for a three-dimensional, primitive equation, numerical ocean model. *Program in Atmospheric and Oceanic Sciences*, Princeton University, Princeton, NJ, 08544-0710.

[99] Mellor, G. L., & Yamada, T. (1974). A hierarchy of turbulence closure models for planetary boundary layers. *Journal of the Atmospheric Sciences*, 31(7), 1791-1806.

[100] Mellor, G. L. (2001). One-dimensional, ocean surface layer modeling: a problem and a solution. *Journal of Physical Oceanography*, 31(3), 790-809.

[101] Oey, L. Y. (2005). A wetting and drying scheme for POM. *Ocean Modelling*, 9(2), 133-150.

[102] Oey, L. Y. (2006). An OGCM with movable land-sea boundaries. *Ocean Modelling*, 13(2), 176-195.

[103] Chen, C., Liu, H., & Beardsley, R. C. (2003). An Unstructured Grid, Finite-Volume, Three-Dimensional, Primitive Equations Ocean Model: Application to Coastal Ocean and Estuaries. *J. Atmos. Oceanic Technol.*, 20, 159-186.

[104] Wright, L. D., Boon, J. D., Xu, J. P., & Kim, S. C. (1992). The bottom boundary layer of the bay stem plains environment of lower Chesapeake Bay. *Estuarine, Coastal and Shelf Science*, 35(1), 17-36, doi: 10.1016/S0272-7714(05)80054-X.

[105] Mehta, A. J. (1988). Laboratory studies on cohesive sediment deposition and erosion. *in Physical processes in estuaries, edited by J. Dronkers and W.V. Leussen*, Springer Verlag, Berlin, 427-445.

[106] Mazda, Y., Magi, M., Kogo, M., & Hong, P. N. (1997). Mangroves as a coastal protection from waves in the Tong King delta, Vietnam. *Mangroves and salt marshes*, 1(2), 127-135, doi: 10.1023/a:1009928003700.

[107] Lee, C. M., Askari, F., Brook, J., Carniel, S., Cushman-Rosin, B., Dorman, C., Doyle, J., Flament, P., Harris, C. K., Jones, B. H., Kuzmic, M., Martin, P., Ogston, A., Orlic, M., Perkins, H., Poulain, P., Pullen, J., Russo, A., Sherwood, C., Signell, R. P., & Thaler, Detweiler. D. (2005). Northern Adriatic response to a wintertime Bora wind event. *EOS Transactions*, 86(16), 19.

[108] Pullen, J., Doyle, J. D., Hodur, R., Ogston, A., Book, J. W., Perkins, H., & Signell, R. (2003). Coupled ocean-atmosphere nested modeling of the Adriatic Sea during winter and spring 2001. *Journal of Geophysical Research*, 108, C103320.

[109] Signell, R. P., Carniel, S., Cavaleri, L., Chiggiato, J., Doyle, J., Pullen, J., & Sclavo, M. (2005). Assessment of operational wind models for the Adriatic Sea using wind and wave observations: a first analysis focused on the Venice lagoon region. *Journal of Marine System*, 53, 217-233.

[110] Matteucci, G., & Frascari, F. (1997). Fluxes of suspended materials in the north Adriatic Sea (Po Prodelta area). *Water, Air and Soil Pollution*, 99, 557-572.

[111] Boldrin, A., Langone, L., Miserocchi, S., Turchetto, M., & Acri, F. (2005). Po River plume on the Adriatic continental shelf: dispersion and sedimentation of dissolved and suspended matter during different river discharge rates. *Marine Geology*, 222-223, 135-158.

[112] Traykovski, P., Wiberg, P. L., & Geyer, W. R. (2006). Observations and modeling of wave-supported sediment gravity flows on the Po prodelta and comparison to prior observations from the Eel shelf. *Continental Shelf Research*, 111, C03S17, doi: 10.1029/2005JC003110.

[113] Grant, W. D., & Madsen, O. S. (1979). Combined wave and current interaction with a rough bottom. *Journal of Geophysical Research*, 84, 1797-1808.

[114] Huisman, J., Von Oostveen, P., & Weissing, F. J. (1999). Critical depth and critical turbulence: two different mechanism for the development of phytoplankton blooms. *Limnology and Oceanography*, 44, 1781-1787.

[115] Gran, H. H., & Braarud, T. (1935). A quantitative study of the phytoplankton in the Bay of Fundy and the Gulf of Marine. *Journal of the Biological Board of Canada*, 1, 279-467.

[116] Sverdrup, H. U. (1953). On conditions for vernal blooming of phytoplankton. *Journal du Conseil- Conseil International Pour L'exploration de La Mer*, 18, 287-295.

[117] Cloern, J. E. (1991). Tidal stirring and phytoplankton bloom dynamics in an estuary. *Journal of Marine Research*, 49, 203-221.

[118] Wang, X. H., Oddo, P., & Pinardi, N. (2006). On the bottom density plume on coastal zone off Gargano (Italy) in the southern Adriatic Sea and its inter-annual variability. *Journal of Geophysical Research*, 111, C03S17, doi:10.1029/2005JC003110.

[119] Palinkas, C. M., Nittrouer, C. A., Wheatcroft, R. A., & Langone, L. (2005). The use ^{7}Be to identify event and seasonal sedimentation near the Po River delta, Adriatic Sea. *Marine Geology*, 222-223, 95-112.

IntechOpen